NUKLEONIKA 2015;60(1):121–126
doi: 10.1515/nuka-2015-0025

ORIGINAL PAPER

DE GRUYTER
OPEN

Hyperfine interaction and some thermomagnetic properties of amorphous and partially crystallized $Fe_{70-x}M_xMo_5Cr_4Nb_6B_{15}$ (M = Co or Ni, x = 0 or 10) alloys

Jakub Rzącki, Jan Świerczek, Mariusz Hasiak, Jacek Olszewski, Józef Zbroszczyk, Wanda Ciurzyńska

Abstract. As revealed by Mössbauer spectroscopy, replacement of 10 at.% of iron in the amorphous $Fe_{70}Mo_5Cr_4Nb_6B_{15}$ alloy by cobalt or nickel has no effect on the magnetic structure in the vicinity of room temperature, although the Curie point moves from 190 K towards ambient one. In the early stages of crystallization, the paramagnetic crystalline $Cr_{12}Fe_{36}Mo_{10}$ phase appears before α-Fe or α-FeCo are formed, as is confirmed by X-ray diffractometry and transmission electron microscopy. Creation of the crystalline $Cr_{12}Fe_{36}Mo_{10}$ phase is accompanied by the amorphous ferromagnetic phase formation at the expense of amorphous paramagnetic one.

Key words: Mössbauer spectroscopy • amorphous alloys • magnetic properties • X-ray diffraction • Curie temperature

J. Rzącki✉, J. Świerczek, J. Olszewski, J. Zbroszczyk, W. Ciurzyńska
Institute of Physics,
Czestochowa University of Technology,
19 Armii Krajowej Ave., 42-200 Częstochowa, Poland,
Tel./Fax: +48 34 325 0795,
E-mail: jrzacki@wip.pcz.pl

M. Hasiak
Department of Mechanics and Material Science,
Wrocław University of Technology,
25 Smoluchowskiego Str., 50-370 Wrocław, Poland

Received: 18 June 2014
Accepted: 25 October 2014

Introduction

Amorphous alloys are usually multicomponent systems with high glass-forming ability. The binary magnetic amorphous alloys consisting of one magnetic compound and the other non-magnetic are the simplest system. The amorphous alloys do not exhibit long-range order of atoms and only topological and chemical short-range order exists in them [1]. The preparation of amorphous metal–metalloid ribbons requires high-quenching rates (10^4–10^6 K/s), which causes instability of quenching process and in turn, leads to the compositional and topological inhomogeneities of the amorphous alloys. The amorphous state is thermodynamically instable and through several metastable states tends to the crystalline one. The crystallization process may occur even at relatively low temperature. This process depends on annealing conditions and the chemical composition of alloys, and may take place in one or several stages [2]. Mössbauer spectroscopy may be used to determine the Fe environments characterizing microstructure and magnetic evolution of both amorphous and crystalline phases. The Mössbauer spectra of partially crystallized alloys are more complex than those of fully amorphous materials. In the crystalline or partially crystallized alloys, Mössbauer spectroscopy is usually used for identification of crystalline phases [3]. In the case of non-magnetic phases occurring in the alloys, the complementary techniques such as X-ray diffractometry or/and transmission electron microscopy have to be applied.

The influence of the composition and thermal treatments on hyperfine parameters and Curie temperature of multicomponent $Fe_{70-x}M_xMo_5Cr_4Nb_6B_{15}$ (M = Co or Ni, x = 0 or 10) alloys containing one or two kinds of magnetic elements and three kinds of late-transition metals was investigated.

Experimental procedure

Ribbons of $Fe_{70-x}M_xMo_5Cr_4Nb_6B_{15}$ (M = Co or Ni, x = 0 or 10) alloys of 20 μm thickness and 10 mm width were obtained by the melt-spinning technique under an argon atmosphere. In order to determine the temperatures of the heat treatment, different scanning calorimetry (DSC) curves were recorded using a differential scanning calorimeter with a heating rate of 10 K/min. The microstructure and magnetic order were studied by Mössbauer spectroscopy. Transmission Mössbauer spectra were recorded at the temperature equal to 308 K using a standard spectrometer with constant acceleration and ^{57}Co(Rh) source of 50 mCi radioactivity. The Mössbauer spectra were fitted using the Normos package [3]. Additionally, the microstructure was studied by X-ray diffractometry and transmission electron microscopy. A Bruker-AXS, type D8 Advanced X-ray diffractometer and a JEM 3010 microscope working at high-resolution regime were used. The magnetization curves were measured in the temperature range 50–400 K and in magnetizing field induction 5 mT by a VersaLab (Quantum Design) system. All investigations were carried out for the as-quenched and annealed samples. The samples were cut out from the amorphous ribbons and subjected to annealing for 30 min at one chosen temperature. Because we wish to deal with the primary crystallization, the temperatures of the heat treatment are chosen within temperature ranges: 600–915 K, 600–905 K and 600–1185 K for the amorphous $Fe_{70}Mo_5Cr_4Nb_6B_{15}$, $Fe_{60}Co_{10}Mo_5Cr_4Nb_6B_{15}$ and $Fe_{60}Ni_{10}Mo_5Cr_4Nb_6B_{15}$ alloys, respectively.

Results and discussion

In Fig. 1 the exemplary DSC curve obtained at heating rate of 10 K/min for the as-quenched amorphous $Fe_{70}Mo_5Cr_4Nb_6B_{15}$ alloy is depicted. Two well-separated dips corresponding to the primary and secondary crystallization are visible. The exothermic dip related to the primary crystallization is broad and shallow. It means that the primary crystallization can take place at a wide range of temperatures and starts at about 800 K. Similar behavior is observed for Co containing alloy, whereas the onset of primary crystallization for the alloy with Ni is at about 1125 K.

X-ray diffraction pattern for the as-quenched amorphous $Fe_{60}Co_{10}Mo_5Cr_4Nb_6B_{15}$ alloy and its evolution with the annealing temperature are shown in Fig. 2. The typical pattern for the amorphous structure with two broad diffraction maxima in the as-quenched state exhibits no distinct changes after annealing at 600 K for 30 min. The well-visible

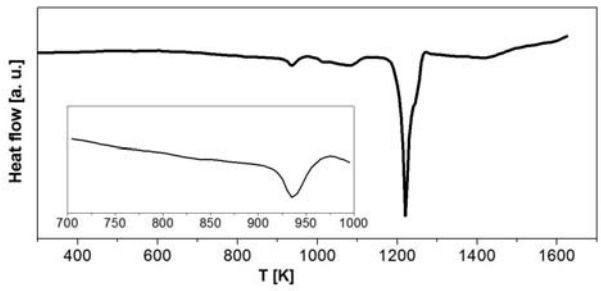

Fig. 1. DSC curve obtained at the heating rate of 10 K/min for the amorphous $Fe_{60}Co_{10}Mo_5Cr_4Nb_6B_{15}$ alloy. The magnified dip of the primary crystallization is displayed as an inset.

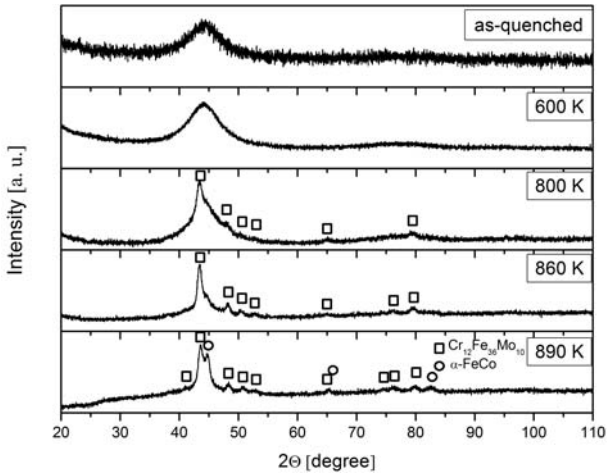

Fig. 2. X-ray diffraction patterns for the as-quenched and annealed $Fe_{60}Co_{10}Mo_5Cr_4Nb_6B_{15}$ alloy. The peaks corresponding to the crystalline $Cr_{12}Fe_{36}Mo_{10}$ and α-FeCo phases are denoted in the figure.

sharpening of the main diffraction 'hallo' and some additional peaks appear after annealing at 800 K and

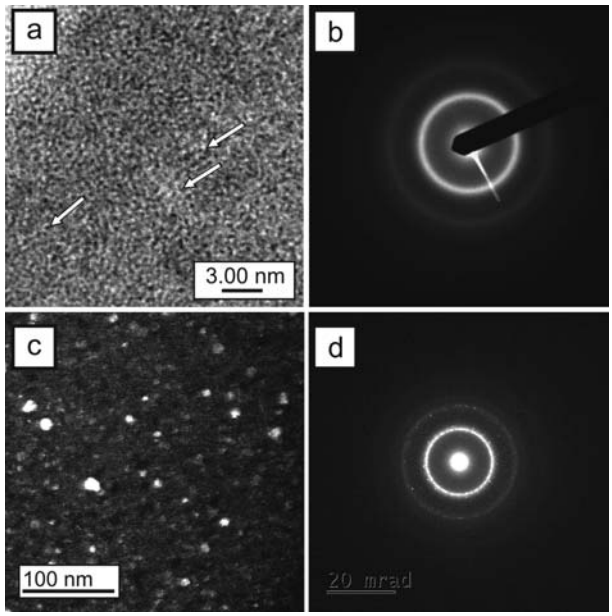

Fig. 3. The transmission electron-microscopy images and electron-diffraction patterns for $Fe_{60}Co_{10}Mo_5Cr_4Nb_6B_{15}$ alloy in the as-cast state (a, b) and after the annealing at 800 K for 30 min (c, d). The visible medium-range ordering regions are denoted by arrows.

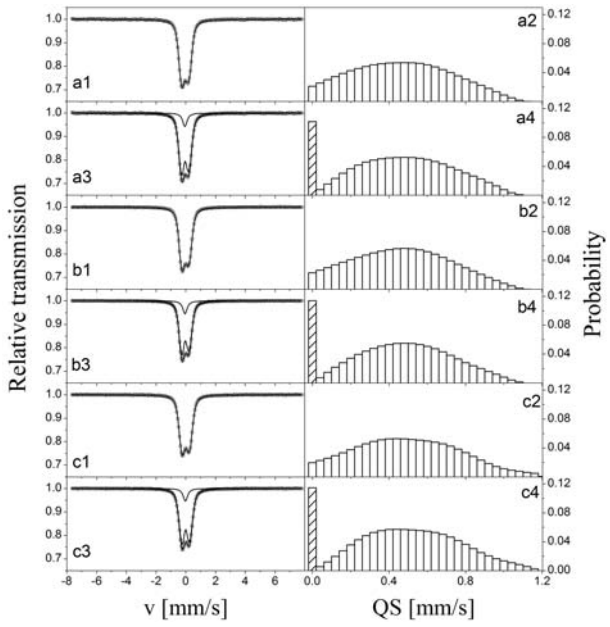

Fig. 4. Transmission Mössbauer spectra and corresponding QS distributions for the as-quenched $Fe_{70}Mo_5Cr_4Nb_6B_{15}$ (a1, a2), $Fe_{60}Co_{10}Mo_5Cr_4Nb_6B_{15}$ (b1, b2) and $Fe_{60}Ni_{10}Mo_5Cr_4Nb_6B_{15}$ (c1, c2) amorphous alloys using one block of symmetric quadrupole distributions, and the decomposition into a single line and a block of symmetric quadrupole distributions for the as-quenched $Fe_{70}Mo_5Cr_4Nb_6B_{15}$ (a3, a4), $Fe_{60}Co_{10}Mo_5Cr_4Nb_6B_{15}$ (b3, b4) and $Fe_{60}Ni_{10}Mo_5Cr_4Nb_6B_{15}$ (c3, c4) amorphous alloys.

are more pronounced with the increase of annealing temperature. Their positions and the inter-plane distances indicate that they belong to the crystalline $Cr_{12}Fe_{36}Mo_{10}$ phase. With the increase of annealing temperature in X-ray diffraction, pattern peaks ascribed to α-FeCo phase appear. Similar behavior is observed for the $Fe_{70}Mo_5Cr_4Nb_6B_{15}$ alloy, whereas the crystallization starts in Ni-containing alloy during annealing at 1000 K. The presence of this granular phase is also confirmed by the transmission electron microscopy. In Fig. 3 the bright-field electron images and corresponding electron-diffraction patterns for the amorphous $Fe_{60}Co_{10}Mo_5Cr_4Nb_6B_{15}$ alloy in the as--cast state and after annealing at 800 K for 30 min are presented. Structures ascribed to the medium--range ordering regions are assigned by white arrows regions. In the high-resolution image for the as-cast ribbons, the fringe like regions can be distinguished [4], whereas the electron-diffraction pattern is characteristic of amorphous state (Fig. 3a,b). After annealing at 800 K for 30 min, the crystalline grains embedded in amorphous remainder can be observed (Fig. 3c) that are accompanied by the bright spots observed on the diffraction rings (Fig. 3d). Their position confirms that they belong to the above--mentioned crystalline phase.

Transmission Mössbauer spectra of the as--quenched $Fe_{70}Mo_5Cr_4Nb_6B_{15}$, $Fe_{60}Co_{10}Mo_5Cr_4Nb_6B_{15}$ and $Fe_{60}Ni_{10}Mo_5Cr_4Nb_6B_{15}$ alloys and corresponding quadrupole splitting distributions P(QS) are depicted in Fig. 4. The spectra in the form of asymmetric doublets are characteristic of amorphous paramagnets (Fig. 4a1,b1,c1) with the QS distribution obtained on the assumption that the linear dependence of isomer shift on QS exists (Fig. 4a2, b2,c2). Not vanishing probability for QS = 0 can be ascribed to Fe sites with cubic symmetry of nearest neighborhood. According to this, the best fitting is obtained when the spectrum is decomposed into a single line and a component with QS distribution (Fig. 4a3,a4,b3,b4,c3,c4). Some fitted hyperfine parameters are listed in Table 1. It is seen that the relative intensities of components and the average QS for all investigated samples in the as-quenched state are similar. In Fig. 5, Mössbauer spectra and related hyperfine parameters distribution for the $Fe_{60}Co_{10}Mo_5Cr_4Nb_6B_{15}$ alloy subjected to the annealing at 600, 800, 860 and 890 K for 30 min are shown. No distinct changes in spectra and P(QS)

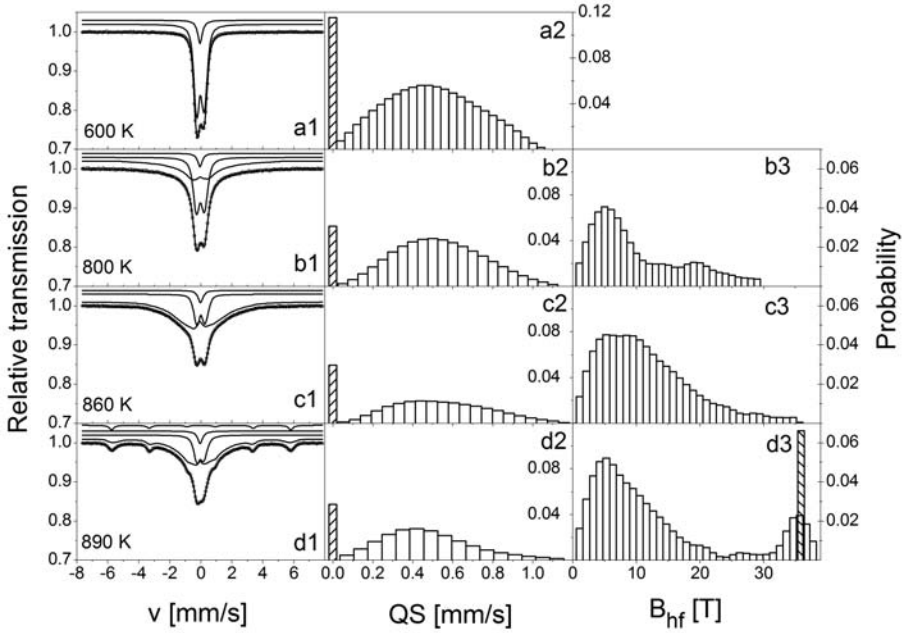

Fig. 5. Transmission Mössbauer spectra (a1, b1, c1, d1) and corresponding QS (a2, b2, c2, d2) and hyperfine field induction (b3, c3, d3) distributions for the annealed $Fe_{60}Co_{10}Mo_5Cr_4Nb_6B_{15}$ alloy.

Table 1. Some fitted hyperfine parameters of the spectra decomposition shown in Figs. 4–7 of components originating from amorphous paramagnetic, amorphous ferromagnetic, α-Fe and α-FeCo crystalline phases for the $Fe_{70-x}M_xMo_5Cr_4Nb_6B_{15}$ (M = Co or Ni, x = 0 or 10) alloys in the as-quenched state and after annealing: IS_L – the average value of IS for a single line, A_S – the relative area of a single line, $\overline{QS}$ – the mean value of the quadrupole splitting, A_{AP} – the relative area of the amorphous paramagnetic component, $\bar{B}_{hf}$ – the average value of the hyperfine field induction for amorphous ferromagnetic component, A_{AF} – the relative area of the amorphous ferromagnetic component, B_{cr} – the hyperfine field induction for the crystalline phase, A_{cr} – the relative area for the crystalline phase. Statistical uncertainties for the significant figure are given in brackets

Thermal history of the sample	IS_L [mm/s]	A_{SL} [%]	$\overline{QS}$ [mm/s]	A_{AP} [%]	$\bar{B}_{hf}$ [T]	A_{AF} [%]	B_{cr} [T]	A_{cr} [%]
$Fe_{70}Mo_5Cr_4Nb_6B_{15}$ as-quenched	−0.053(3)	10	0.50(5)	90				
annealed at 600 K	−0.066(3)	11	0.50(5)	89				
annealed at 800 K	−0.078(3)	13	0.49(5)	87				
annealed at 905 K	−0.061(3)	19	0.44(5)	66	17(1)	15		
annealed at 915 K	−0.219(3)	17	0.46(5)	50	16(1)	20	33.2(2)	13
$Fe_{60}Co_{10}Mo_5Cr_4Nb_6B_{15}$ as-quenched	−0.053(2)	11	0.50(5)	89				
annealed at 600 K	−0.054(2)	12	0.50(5)	88				
annealed at 800 K	−0.057(8)	5	0.53(5)	51	10(1)	46		
annealed at 860 K	−0.020(2)	5	0.57(5)	24	12(1)	71		
annealed at 890 K	−0.058(6)	5	0.45(5)	31	19(1)	54	35.91(3)	10
$Fe_{60}Ni_{10}Mo_5Cr_4Nb_6B_{15}$ as-quenched	−0.025(2)	10	0.53(5)	90				
annealed at 600 K	−0.023(3)	7	0.52(5)	93				
annealed at 800 K	−0.016(2)	11	0.51(5)	73	10(1)	16		
annealed at 1125 K	−0.075(2)	15	0.21(5)	21	10(1)	64		
annealed at 1185 K	−0.186(4)	17	0.22(5)	43	24(1)	32	33.80(5)	8

distributions after annealing at 600 are observed compared to the as-quenched state. It is noteworthy that after annealing at 800 K, the crystalline $Cr_{12}Fe_{36}Mo_{10}$ phase appears in the matrix as is indicated by X-ray diffractometry. It is seen that this phase does not contribute to the overall spectrum in the form of a sextet of Lorentzian lines but as a single line. Moreover, after this annealing, the amorphous ferromagnetic phase can be distinguished in the spectrum decomposition (Fig. 5c1–3). The contribution of this component increases with annealing temperature (Fig. 5d1–3) at the expense of the amorphous paramagnetic phase (Fig. 5c2–3, Table 1). After the heat treatment at 890 K, apart from the subspectra related to the paramagnetic crystalline $Cr_{12}Fe_{36}Mo_{10}$ phase, paramagnetic and ferromagnetic amorphous phases, the component ascribed to the crystalline grains of α-FeCo phase occur in the sample (Fig. 5d1–3, Table 1). The ferromagnetic amorphous phase is described by B_{hf} distribution assuming the linear dependence of IS on B_{hf} and QS = 0 for each sextet. Similar behavior is observed for $Fe_{70}Mo_5Cr_4Nb_6B_{15}$ alloy but only the very small amount of ferromagnetic amorphous phase appears after annealing at 905 K (Fig. 6c1–3). Transmission Mössbauer spectra and

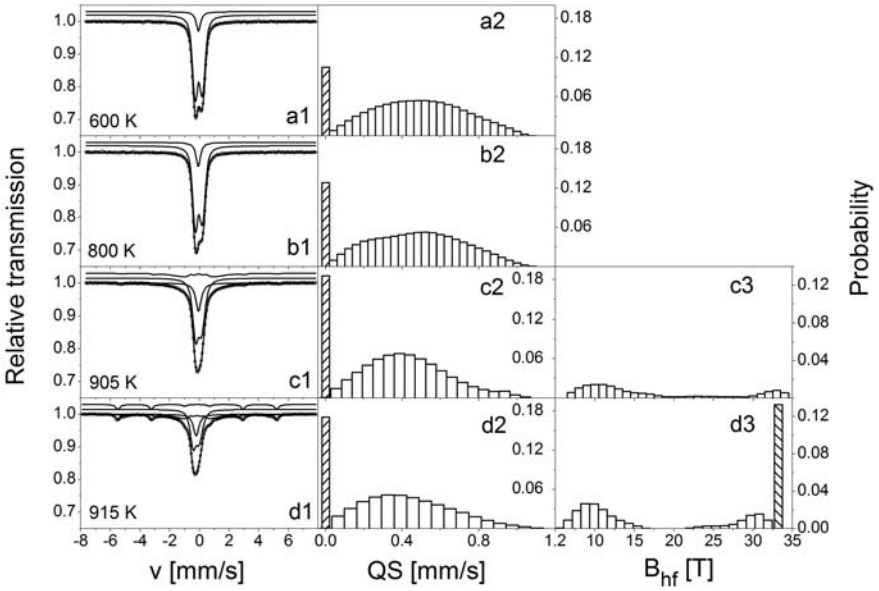

Fig. 6. Transmission Mössbauer spectra (a1, b1, c1, d1) and corresponding QS (a2, b2, c2, d2) and hyperfine field induction (c3, d3) distributions for the annealed $Fe_{70}Mo_5Cr_4Nb_6B_{15}$ alloy.

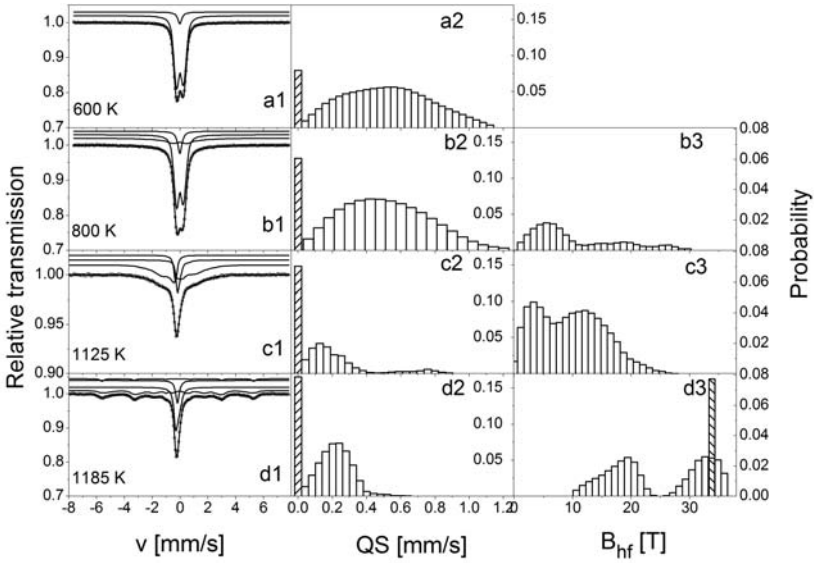

Fig. 7. Transmission Mössbauer spectra (a1, b1, c1, d1) and corresponding QS (a2, b2, c2, d2) and hyperfine field induction (c3, d3) distributions for the annealed $Fe_{60}Ni_{10}Mo_5Cr_4Nb_6B_{15}$ alloy.

corresponding hyperfine parameters distributions for the $Fe_{60}Ni_{10}Mo_5Cr_4Nb_6B_{15}$ alloy subjected to the heat treatments at 600, 800, 1125 and 1185 K are depicted in Fig. 7. After annealing at 600 K, only very small changes in spectra and their decompositions are observed compared to the previously discussed alloys. The distinct broadening of the overall spectrum is observed after annealing at 1125 K, whereas, the crystalline α-Fe phase is visible for the samples annealed at 1185 K (Fig. 7d1,d3; Table 1). The specific magnetization vs. temperature and the derivative *dM/dT* numerically calculated (as an inset) for the as-quenched amorphous samples are presented in Fig. 8. The *dM/dT* curves of the annealed alloys (Fig. 9, inset), compared to the as-quenched state, exhibit broad maximum connected with inhomogeneities occurring in the samples. It is in good agreement with the results obtained from Mössbauer spectroscopy (Figs. 5–7, Table 1). The temperatures of maxima equal to 354 K (for $Fe_{60}Co_{10}Mo_5Cr_4Nb_6B_{15}$ alloy annealed at 860 K) and 338 K (for $Fe_{60}Ni_{10}Mo_5Cr_4Nb_6B_{15}$ annealed at 1125 K) correspond to the Curie points of amorphous phases ferromagnetic at room temperature. However, in the case of $Fe_{70}Mo_5Cr_4Nb_6B_{15}$ alloy annealed at 800 K for 30 min, no contribution of the amorphous ferromagnetic phase to Mössbauer spectrum is seen (Fig. 6c1,c3) and the temperature of maximum 191 K can be treated as the Curie temperature of the phase paramagnetic at room one, at least partially relaxed.

Conclusions

– Substitution of 10 at.% of iron by Co or Ni in the amorphous $Fe_{70}Mo_5Cr_4Nb_6B_{15}$ alloy preserves paramagnetic state at room temperature as is stated from Mössbauer spectroscopy studies.

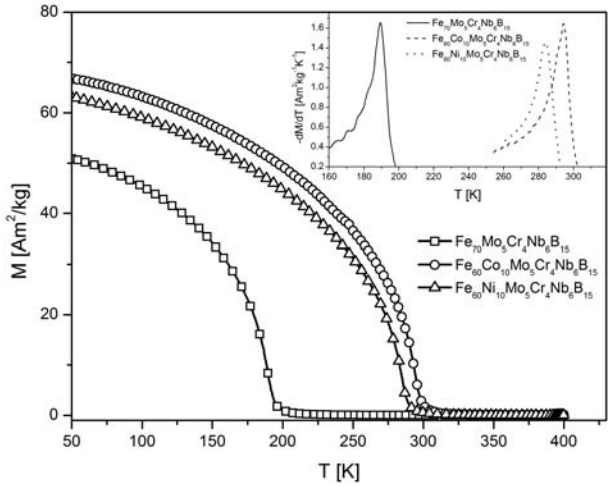

Fig. 8. The specific magnetization (*M*) vs. temperature for the as-quenched amorphous $Fe_{70}Mo_5Cr_4Nb_6B_{15}$, $Fe_{60}Co_{10}Mo_5Cr_4Nb_6B_{15}$ and $Fe_{60}Ni_{10}Mo_5Cr_4Nb_6B_{15}$ alloys measured at the magnetizing field induction of 5 mT. To obtain the Curie temperatures the derivatives *dM/dT* on temperature as an inset are depicted.

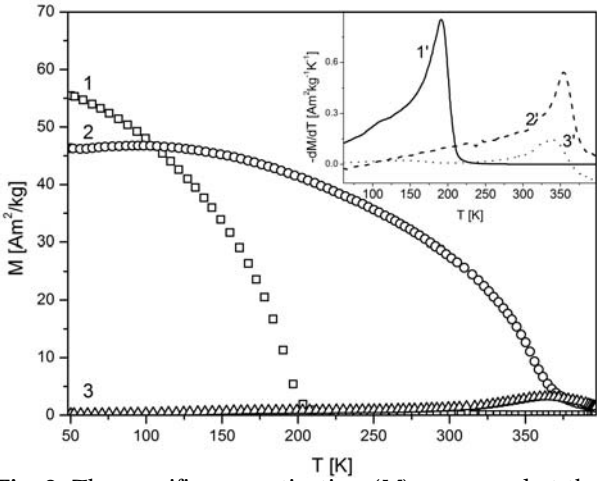

Fig. 9. The specific magnetization (*M*), measured at the magnetizing field induction of 5 mT, vs. temperature and the derivative *dM/dT* on temperature, as an inset, for the annealed: at 800 K $Fe_{70}Mo_5Cr_4Nb_6B_{15}$ (1, 1'), at 860 K $Fe_{60}Co_{10}Mo_5Cr_4Nb_6B_{15}$ (2, 2') and at 1125 K $Fe_{60}Ni_{10}Mo_5Cr_4Nb_6B_{15}$ (3, 3') alloys.

- The addition of Co has no distinct effect on early stages of crystallization. The paramagnetic crystalline $Cr_{12}Fe_{36}Mo_{10}$ phase is observed after annealing at the same temperature (800 K) as in the case of $Fe_{70}Mo_5Cr_4Nb_6B_{15}$ alloy. On the contrary, the replacement of 10% of iron atoms by Ni increases the temperature of early stages of crystallization and that phase appears after annealing at 1000 K.
- Except for the crystalline $Cr_{12}Fe_{36}Mo_{10}$, during the heat treatment of investigated alloys, the amorphous ferromagnetic phase is created at the expense of paramagnetic amorphous one.
- The Curie points for the amorphous $Fe_{70}Mo_5Cr_4Nb_6B_{15}$, $Fe_{60}Co_{10}Mo_5Cr_4Nb_6B_{15}$ and $Fe_{60}Ni_{10}Mo_5Cr_4Nb_6B_{15}$ alloys in the as-quenched state are equal to 190, 295 and 283 K, respectively, and depend on annealing conditions.
- Due to structural transformation of amorphous paramagnetic and ferromagnetic phases the crystalline α-Fe or α-FeCo grains grow.

References

1. Brüning, R., Altounian, Z., & Ström-Olsen, J. O. (1987). Reversible structural relaxation in Fe-Ni-B-Si metallic glasses. *J. Appl. Phys*., *62*, 3633–3638. DOI: 10.1063/1.339267.
2. McHenry, M. C., Willard, M. A., & Loughlin, D. E. (1999). Amorphous and nanocrystalline materials for applications as soft magnets. *Prog. Mater. Sci*., *44*, 291–433, and references therein. DOI: 10.1016/S0079-6425(99)00002-X.
3. Brand, R. A. (1987). Improving the validity of hyperfine field distributions from magnetic alloys. *Nucl. Instrum. Methods Phys. Res. Sect. B-Beam Interact. Mater. Atoms*, *28*, 398–416. DOI: 10.1016/0168-583X(87)90182-0.
4. Świerczek, J. (2010). Medium range ordering and some magnetic properties of amorphous $Fe_{90}Zr_7B_3$ alloy. *J. Magn. Magn. Mater*., *322*, 2696–2702. DOI: 10.1016/j.jmmm.2010.04.010.